ROUGHNESS MEASUREMENT FROM MULTI-STEREO RECONSTRUCTION

Benoît Petitpas[1,2], Laurent Beaudoin[3], Michel Roux[1], Jean-Paul Rudant[2]

[1] Institut Telecom, Telecom ParisTech, CNRS UMR 5141 LTCI
46, rue Barrault 75634 Paris Cedex 13, France
michel.roux@telecom-paristech.fr
http://www.ltci.enst.fr
[2] Equipe GTMC (Géomatique, Télédétection, Modélisation des Connaissances)
Universit de Paris-Est-Marne-La-Valle
Bd Descartes,Champs-sur-marne, Marne-la-Vallée, France
benoit.petitpas@telecom-paristech.fr, jean-paul.Rudant@univ-mlv.fr
[3] Pôle Acquisition et Traitement des Images et du Signal (A.T.I.S.)
École Supérieure dInformatique Électronique Automatique (E.S.I.E.A)
72 avenue Maurice Thorez, 94200 Ivry-sur-Seine, France
beaudoin@esiea.fr

Commission III/3

KEY WORDS: Stereo-vision, point cloud, soil roughness, bundle adjustment, epipolar geometry, auto-calibration

ABSTRACT:

In this paper, a new method for computing surface parameters, especially the surface roughness, is presented. This method is designed for easily reconstruct and extract informations from a collection of photos taken without any constraints. This absence of constraints is possible since camera calibration can be computed with bundle adjustment auto-calibration methods. 3D information can then be retrieved with triangulation techniques from the disparity maps computed for each image pair. This paper proposes a new statistically grounded extraction of the roughness directly on the 3D point cloud. Joining 3D and image processing methods, the roughness can be computed only on certain objects with image segmentation. The results are shown on different datasets proving the method robustness.

1 INTRODUCTION

Soil roughness is a crucial parameter for numerous of tasks: radar image analysis is particularly interested in surfaces characterization, roughness being part of the radar backscattered signal (Ulaby et al., 1979), soil erosion from wind or rainfall (van Donk and Skidmore, 2003), hydrologists need also surface roughness for soil moisture measurement (Baghdadi et al., 2008). Many applications are in the field of agriculture studying (Davidson et al., 2000).
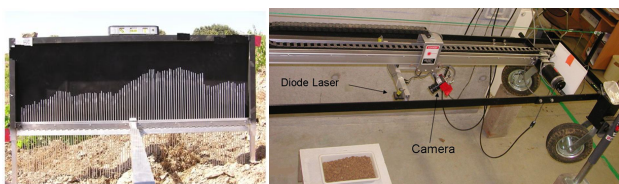

Figure 1: Profilometer

There are various definitions of the roughness parameter. For example the ISO norm 25178, that explains all the roughness parameters you can find in industry and characterization of surface roughness. This is a collection of international standards relating to the analysis of 3D area surface textures.
In radar remote sensing, the standard deviation (SD) of height to surface is computing. People involved in soil dielectric characterization such as (Ulaby et al., 1996) and (Fung et al., 1992) describe roughness as the standard deviation of height, the correlation length and the auto-correlation function(ACF) along transects.

Unfortunately the soil roughness, which appears as a crucial parameter, is really difficult to extract. Nowadays two methods are used (Verhoest et al., 2008) as seen in Figure 1. The first one consists in an horizontal stick with a metal pin every centimeters, then the sticks are moved over the studied surface with a regular displacement step. The problems with this technique are, that the resulting resolutions are not the same between pins and displacement, that it is hard to find the level, that the pins are crushing herbs and small vegetation, difficulties to know the position of acquisition if you do not use another device, GPS or tachymeter. It is a slow technique and it is really hard to find reliable data. The second technique uses a laser(LIDAR) for acquiring a profile with a previous calibration. The advantage of the laser is to be more precise vertically than the pin profilometer (Jester and Klik, 2005), but it needs competent people and is more expensive.
Therefore it would be important to find a new method for extracting surface roughness without heavy constraints as it exists. Retrieving surface could be performed with computer vision techniques which allow to compute roughness only from an image collection.

In order to do measurements on point cloud acquired by stereovision, a calibration is needed either by using calibration targets either using auto-calibration methods. Techniques appear for auto-calibrated a camera system (Pollefeys et al., 1999a), (Triggs et al., 1999) with uncertainties. The bundle adjustment technique offers a good calibration compare to classical approaches (Triggs, 1997) using Kruppa equations resolution. Bundle adjustment allows to take images without strong positioning constraints.
The possibility to take a large number of images and the development of epipolar geometry, auto-calibration and robust matching have permitted from unconstrained pictures to generate automatically 3D point cloud as it will be explain in section 2.
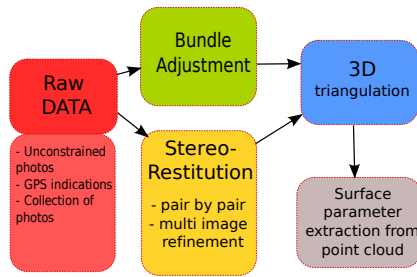
Figure 2: Pipeline of algorithm

From that cloud is extracted roughness measurement with classical methods as it will be explained in Section 3. Then the results and possible improvements will be discuss in Section 4.

2   VISION PIPELINE

This section develops the algorithms used for retrieving a 3D point cloud from images. From raw images, it explains how calibration is computed, disparity map founded and eventually how the triangulation is performed to retrieve the 3D data. The Figure 3 depicts the various algorithms used to find 3D point cloud from stereo images.
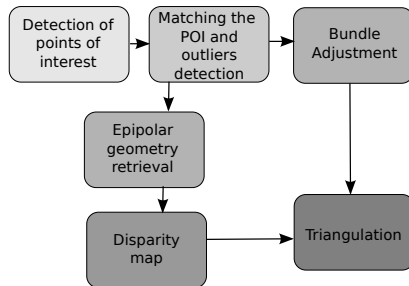

Figure 3: Pipeline of the Disparity map creation

2.1   Data

Raw data consists in images taken with a camera without any constraints on the positioning or on the focal length.

In this paper two set of data are used, the first one is a set of pebble images sensed almost vertically, taken at the Parc des Tuileries, in Paris, the set corresponds to a 10 centimeter square surface and 20 pictures were taken. The second is a set of images of a bonzaï taken with a perspective angle, and corresponds to a set of 14 images. All of these pictures were taken by a hand-held standard camera and without constraint on position, scale or rotation.

2.2   SIFT

Robust correspondences between the images are needed for retrieving the calibration and computing the disparity map. The development of the SIFT (Lowe, 1999) permits to be robust to scale changes.

SIFT algorithm detects and describes local features in images. It is based on scale-space extrema detection on difference of Gaussian. It eliminates edge corresponding points. It affects numbers of local Gaussian descriptors of keypoint to every of them which will be helpful for the matching step. The correspondences are computed with a simple ℓ_2 norm between two descriptors. For

being robust to any bad correspondences, a step of outliers detection is essential. Techniques using robust estimator such as RANSAC permits to be confident in the matches
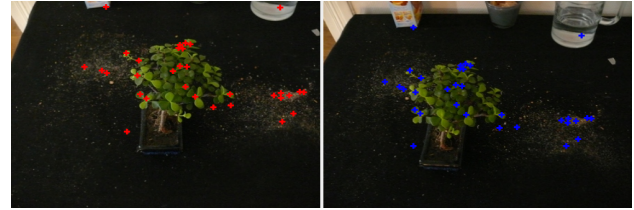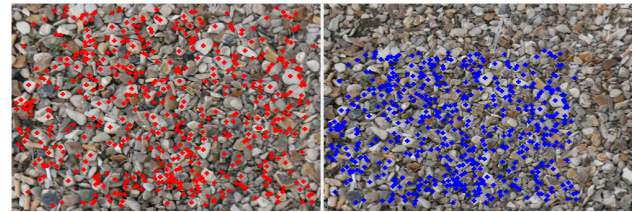

Figure 4: SIFT matching on Bonzaï image

Figure 5: SIFT matching on pebble image at different scale

SIFT keypoints are invariant to scale but not to rotation or perspective projection. Other techniques such as SURF (Bay et al., 2008) could be part of a future work.

2.3   Bundle Adjustment

Bundle adjustment is a major step of our vision pipeline which computes cameras calibrations from images. This technique was developed in the early 50's in the research field of photogrammetry, and is now commonly used in computer vision.

As it is shown in (Triggs et al., 1999), bundle adjustment consists in simultaneously refining the coordinate of 3D point clouds and the camera parameters, corresponding to the characteristics of the camera (focal length, distortions) and to the motion between the acquisitions. Bundle adjustment find the best set of data that minimizes the distance between the re-projected points on images and the initial position.

Assume that n 3D points are viewed by m cameras. The criterion to minimize is :

$$\min_{P_j, X_i} \sum_{i=1}^{n} \sum_{j=1}^{m} d(P_j . X_i, x_{i,j})^2 \qquad (1)$$

with P_j is the jth camera projection matrix, X_i the ith 3D points and $x_{i,j}$ the image corresponding point, where $P.X$ denotes the projected 3D point in the image and $d(.,.)$ the Euclidean distance. For minimizing this criterion, techniques like Levenberg-Marquardt are usually used (Triggs et al., 1999).

Recently a good implementation was proposed for a collection of photos and distributed under GPL licence (Snavely et al., 2008), based on the work of (Lourakis and Argyros, 2004), which lead us to choose this technique.

Bundle adjustment is considered to be not robust enough. For being more trustful in this procedure, some parameters are prior extracted from the EXIF data and used as initialization, giving us already intrinsic parameters, such as focal length.

In some particular cases, bundle adjustment did not give an enough good result to be used. Other robust techniques are considered

and may be part of future work.

2.4 Epipolar dense stereo reconstruction

After the step of keypoint detection and calibration, images are re-sampled in the same epipolar geometry for finding dense correspondences. Developed in (Faugeras, 1993), the fundamental matrix explains totally the epipolar geometry between two images and is computed from a set of corresponding points. It shows that a point in the first image finds its correspondence along the epipolar line in the second image.

In order to make the generation of a dense disparity map easier, all pairs of images are remaped according to the epipolar geometry for having the epipole at the infinite. The search for the correspondence of a point in the first image is then limited along the same line in the second image. Because of its robustness, the polar epipolar rectification technique (Pollefeys et al., 1999b), (Oram, 2001) has been preferred to the linear rectification (Hartley and Zisserman, 2003).
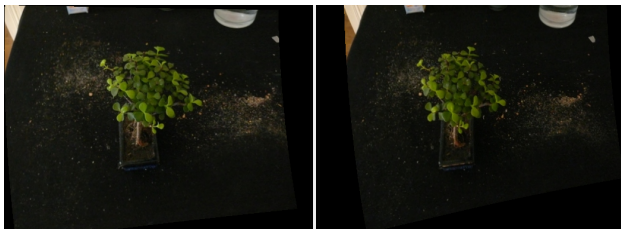

Figure 6: Epipolar rectification of the bonzaï images

Figure 7: Epipolar rectification of the pebble images

Once the rectification process, dense stereo matching is computed with a classical correlation method, such as hierarchical matching with relaxation explained in (Leloglu et al., 1998).
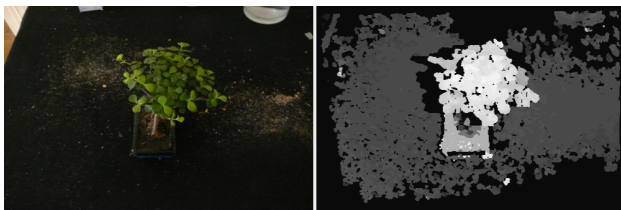

Figure 8: Dense matching on Bonzaï

In order to reduce the stepping effect on the generated surface, a sub-pixel matching refinement is introduced. For each pair of matched pixels, an oversampling of the images with a factor of

Figure 9: Dense matching on pebble

4 is calculated, and a new search is performed in the second image on a 5x5 pixels neighborhood with a 11x11 pixels correlation window.

2.5 Triangulation

The correspondences from all pairs of images can be re-project into the 3D space estimated with the bundle adjustment. The position of a 3D point is calculated by back-projecting two rays from the images and by finding the 3D point that minimize the distance between these two rays. The linear-LS method with a SVD approximation is used as described in (Hartley and Sturm, 1997).
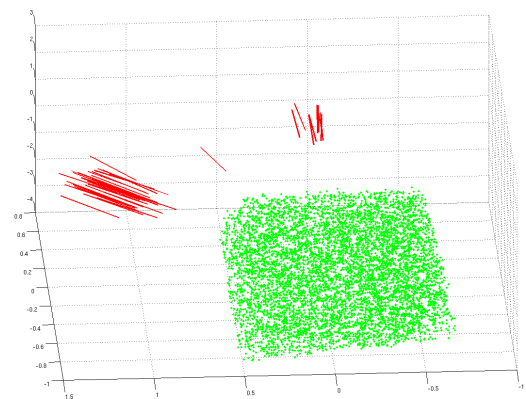

Figure 10: Camera direction on the pebble point cloud

3 ROUGHNESS EXTRACTION

This section introduces the different roughness parameters computed. The most explicit and used parameters of the ISO norm are the root mean square of height (3) and the arithmetical mean of height (4). Remote sensing is also interested in specific parameters explaining the stochastic variation of the soil surface towards a surface reference (Ulaby et al., 1986) and used as input to most backscattered models (Bryant et al., 2007), (Ulaby et al., 1996) : the Standard Deviation (SD) of height (5), the correlation length and the auto-correlation function, the correlation length describes the horizontal distance over which the surface profile is autocorrelated with a value larger than $\frac{1}{e}$ and the auto-correlation function (ACF). Since traditional tools for roughness estimation (profilometer and laser) can sense only profiles, roughness measures are defined accordingly. However, with the 3D point clouds, surface roughness can be estimated spatially and not only along profiles reported as the main source of errors (Bryant et al., 2007). Measurement are carried out relatively to the mean plane Π, computed as the plane that minimizes the distance from

the point cloud to the plane in a least square sense.

$$\Pi = \arg\min_{\pi} \sum_{i=1}^{n} d(p_i, \pi)^2 \qquad (2)$$

Sq : Root mean square of height

$$S_q = \sqrt{\frac{1}{n} \sum_{i=1}^{n} d(p_i, \Pi)^2} \qquad (3)$$

Sa : Arithmetical mean of height

$$S_a = \frac{1}{n} \sum_{i=1}^{n} |d(p_i, \Pi)| \qquad (4)$$

SD : Standard deviation of height

$$SD = \sqrt{\frac{1}{n} \sum_{i=1}^{n} d(p_i, \Pi)^2 - \left(\frac{1}{n} \sum_{i=1}^{n} d(p_i, \Pi)\right)^2} \qquad (5)$$

Where p_i is the ith 3D point, Π the mean plane and $d(.,.)$ the Euclidean distance.

The ACF is calculated along the two directions. The normalized centered ACF of a discrete signal $f_{i,j} = d(p_{i,j}, \pi)$, where π is the mean plane:

$$ACF(k,l) = \frac{\sum_{i=1}^{N-k} \sum_{j=1}^{N-l} (f_{i,j} - \bar{f}).(f_{i+k,j+l} - \bar{f})}{\sum_{i=1}^{N-k} \sum_{j=1}^{N-l} (f_i - \bar{f})^2} \qquad (6)$$

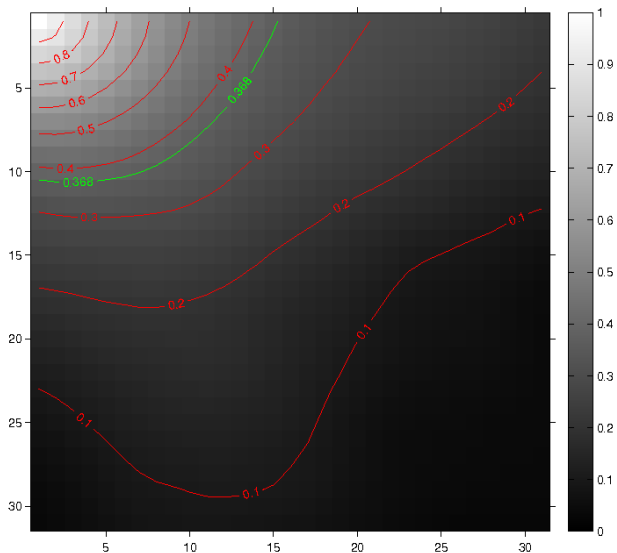where $\bar{f}$ is the mean value of f_i and N is the number of 3D points.

Figure 11: ACF along the two axis for the pebble disparity map, in green the line $1/e$

On figure 11, the ACF of the disparity map generated with the pebble images shows a slight anisotropy of the 3D structure, with a correlation length of 15.5 along the x-axis and 10.5 along the y-axis.

4 RESULTS AND DISCUSSION

In this section, some peculiar results are detailed and several points are discussed. Using stereo-vision instead of profilome-
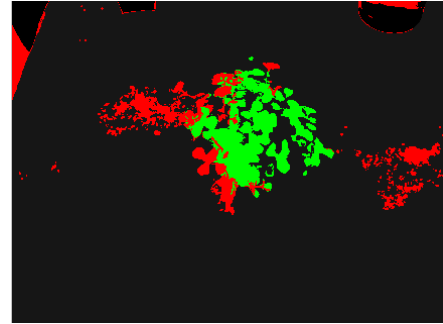

Figure 12: Segmentation on bonzaï

ters offer the possibility to use image processing techniques for helping 3D interpretation. For example using image segmentation focuses the result on the interesting part of the image. In Figure 12 are shown the result on the bonzaï image and below on Table 1 the results of roughness extraction on different segmentation zones.

zone	background	bad segmented zone	entire foliage
Sq	2.95	2.46	1.07
Sa	1.33	1.74	0.62
SD	2.63	1.73	0.87

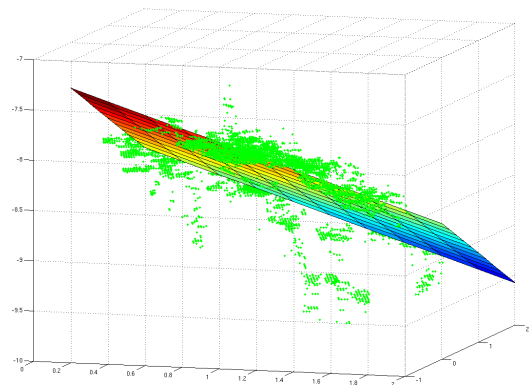Table 1: Sq, Sa and SD in centimeters on the segmented bonzaï

Figure 13: Leaf canopy of Bonzaï and the plan found

The foliage zone is particularly considered, because it is usually difficult to extract information on foliage. It may be helpful for the study of the backscattering signal on forest, and for the estimation of the tree moisture, if roughness of different species are known. On Figure 13 the mean plan of the canopy (the green segmentation zone) is shown. The approach used for segmentation was a colorimetric technique using subsample images implemented in OpenCV, clusters are merged manually if necessary as in the case of the foliage (three clusters merged in one).

The 3D reconstruction uses standard robust methods. The 3D is placed in pixel domain and can be placed in a metric domain by triangulation with a scale factor based on correspondences between pixels and centimeters. A length is selected manually on

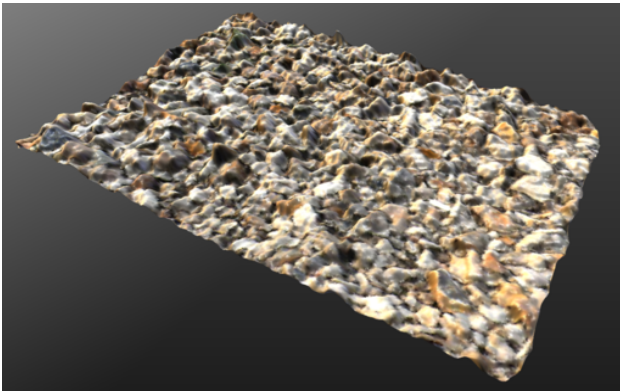Figure 14: 3D view of the pebble with total surface roughness Sq=0.1668029cm, Sa=0.122973cm and SD=0.112528cm

Figure 15: 3D view of the pebble with triangulation

the 3D domain and a relation is establish in centimeter also manually, but because of the uncertainty the pixel domain were preferred. Nevertheless some inaccuracies may occur and generate errors on the corresponding points and on the 3D points location. These errors propagate then to the estimation of the roughness.

Dense matching may be infected by two kind of errors: mismatching and positioning errors. Without a ground truth, the estimation of these errors is very difficult. In order to have an approximation of these errors, we considere the keypoints obtained with the SIFT matching procedure with a sub-pixel accuracy, and calculated the average distance in the second image between the coordinates of the SIFT point and the position found with the correlation process with the oversampling refinement.

As we can see on figure 16, there is no obvious relationship between the correlation error and the estimation of the roughness. Nevertheless, a systematic error of one pixel introduced in the disparity estimation implicates an average error of 0.023 pixel on the 3D point position compared with the original position, which is of the same order as the estimated roughness. This shows the influence of the b/h ration compared to the correlation error.

The errors on auto-calibration are easy to identify but difficult to quantify, because they may arise from outliers of SIFT matchings, or inaccuracies in the Levenberg-Marquardt optimization, even in the data directly found in the meta-data of the image (EXIF), like the focal length. Then, if the calibration is wrong, the estimation of the position of 3D points will not be accurate. To estimate the error of triangulation, we decide to re-project the point cloud in the two images used for creating it. Then the average distance between the points found by back-projection and the original points
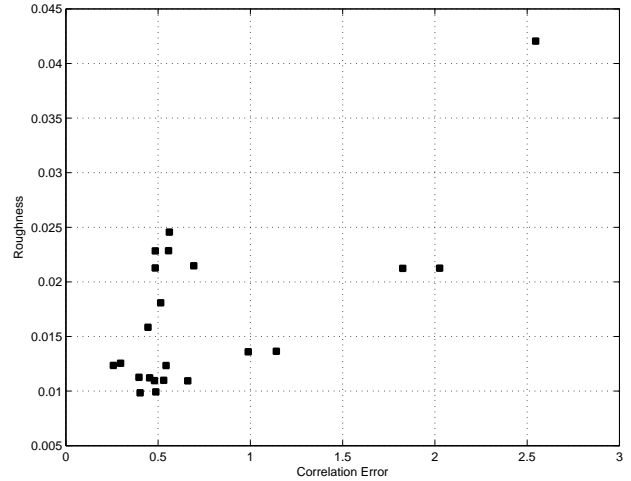

Figure 16: Roughness depending on correlation error

is computed.

$$\varepsilon = \frac{1}{N} \sum_{i=1}^{n} d(P.X_i, x_i)^2 \qquad (7)$$

with P the left camera projection matrix, X_i the ith 3D points and x_i the image corresponding point, where $P.X$ denotes the projected 3D point in the image and $d(.,.)$ the Euclidean distance. The error on the location of the 3D points after the triangulation is resulting from calibration errors. Doing the estimation of 3D point position by triangulation from images with good calibration have shown an average error lower than a quarter of pixel. So the error found on the auto-calibrated images is coming from bad calibration. Figure 17 is showing the impact of calibration error to the SD roughness parameter.
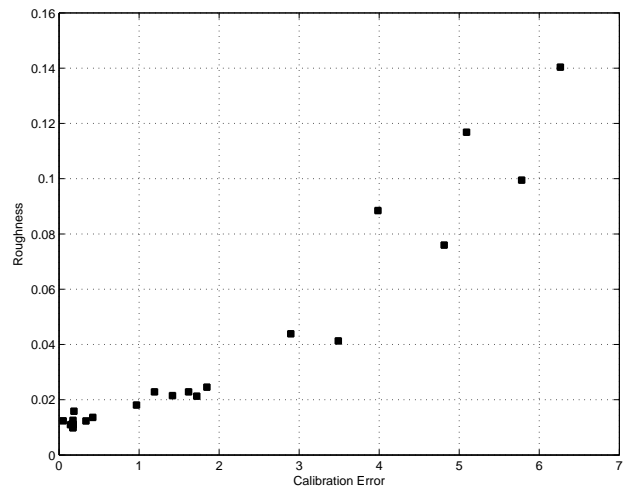

Figure 17: Roughness depending on calibration error

The figure 17 shows that there is a global relationship between the calibration error and the estimation of the roughness. The linear behavior of estimation for a calibration error less than 2 pixels indicates that there is no need to select the only very best calibrated images.

5 CONCLUSIONS AND FUTURE WORK

In this work we propose a new and global approach for extracting soil roughness with unconstraints images. The roughness is di-

rectly extract on a surface and not on profile which is helpful for soil characterization. The surface is computed with stereo-vision techniques and the geometry is retrieved with bundle adjustment. This new method for soil roughness extraction can be applied in radar remote sensing domain as well as in geo-physiques domain as in botanic domain. We estimate the roughness of surface with a precision under the half centimeter, meaning this method is as accurate as pin-profilometer, but is not subject to the same problem. Numerous of other soil parameter can be compute on the 3D point cloud. The accuracy of the 3D reconstruction can be improve. Adding other data like GPS information or calibrated stereo-camera can be a new axis of research.

REFERENCES

Baghdadi, N., Cerdan, O., Zribi, M., Auzet, V., Darboux, F., El Hajj, M. and Kheir, R., 2008. Operational performance of current synthetic aperture radar sensors in mapping soil surface characteristics in agricultural environments: application to hydrological and erosion modelling. Hydrological Processes 22(1), pp. 9–20.

Bay, H., Ess, A., Tuytelaars, T. and Van Gool, L., 2008. Speeded-up robust features (SURF). Computer Vision and Image Understanding 110(3), pp. 346–359.

Bryant, R., Moran, M., Thoma, D., Collins, C., Skirvin, S., Rahman, M., Slocum, K., Starks, P., Bosch, D. and Dugo, M., 2007. Measuring Surface Roughness Height to Parameterize Radar Backscatter Models for Retrieval of Surface Soil Moisture. IEEE Geoscience and Remote Sensing Letters 4(1), pp. 137.

Davidson, M., Le Toan, T., Mattia, F., Satalino, G., Manninen, T. and Borgeaud, M., 2000. On the characterization of agricultural soil roughness for radar remote sensing studies. IEEE Transactions on Geoscience and Remote Sensing 38(2), pp. 630–640.

Faugeras, O., 1993. Three-dimensional computer vision: a geometric viewpoint, MIT Press Ltd.

Fung, A., Li, Z. and Chen, K., 1992. Backscattering from a randomly rough dielectric surface. IEEE Transactions on Geoscience and Remote Sensing 30(2), pp. 356–369.

Hartley, R. and Sturm, P., 1997. Triangulation. Computer Vision and Image Understanding 68(2), pp. 146–157.

Hartley, R. and Zisserman, A., 2003. Multiple view geometry in computer vision. Cambridge Univ Pr.

Jester, W. and Klik, A., 2005. Soil surface roughness measurementmethods, applicability, and surface representation. Catena 64(2-3), pp. 174–192.

Leloglu, M., Roux, M. and Maître, H., 1998. Dense urban DEM with three or more high-resolution aerial images. In: ISPRS Symposium on GIS-Between Visions and Applications. Stuttgart, Germany.

Lourakis, M. and Argyros, A., 2004. The design and implementation of a generic sparse bundle adjustment software package based on the levenberg-marquardt algorithm. ICS/FORTH Technical Report TR.

Lowe, D., 1999. Object recognition from local scale-invariant features. In: International Conference on Computer Vision, Vol. 2, pp. 1150–1157.

Oram, D., 2001. Rectification for any epipolar geometry. In: Proc. British Machine Vision Conf, pp. 653–662.

Pollefeys, M., Koch, R. and Gool, L., 1999a. Self-calibration and metric reconstruction inspite of varying and unknown intrinsic camera parameters. International Journal of Computer Vision 32(1), pp. 7–25.

Pollefeys, M., Koch, R. and Van Gool, L., 1999b. A simple and efficient rectification method for general motion. In: Proc. ICCV99 (international Conference on Computer Vision), pp. 496–501.

Snavely, N., Seitz, S. and Szeliski, R., 2008. Modeling the world from internet photo collections. International Journal of Computer Vision 80(2), pp. 189–210.

Triggs, B., 1997. Autocalibration and the absolute quadric. In: 1997 IEEE Computer Society Conference on Computer Vision and Pattern Recognition, 1997. Proceedings., pp. 609–614.

Triggs, B., McLauchlan, P., Hartley, R. and Fitzgibbon, A., 1999. Bundle adjustment-a modern synthesis. Lecture Notes in Computer Science pp. 298–372.

Ulaby, F., Bradley, G. and Dobson, M., 1979. Microwave backscatter dependence on surface roughness, soil moisture, and soil texture: Part II-vegetation-covered soil. IEEE Transactions on Geoscience Electronics 17(2), pp. 33–40.

Ulaby, F., Dubois, P. and van Zyl, J., 1996. Radar mapping of surface soil moisture. Journal of Hydrology 184(1-2), pp. 57–84.

Ulaby, F., Moore, R. and Fung, A., 1986. Microwave remote sensing: active and passive. Artech House, Norwood, MA.

van Donk, S. and Skidmore, E., 2003. Measurement and simulation of wind erosion, roughness degradation and residue decomposition on an agricultural field. Earth Surface Processes and Landforms 28(11), pp. 1243–1258.

Verhoest, N., Lievens, H., Wagner, W., Álvarez-Mozos, J., Moran, M. and Mattia, F., 2008. On the soil roughness parameterization problem in soil moisture retrieval of bare surfaces from synthetic aperture radar. Sensors 8(7), pp. 4213–4248.